POLARIZED INFRARED SPECTROSCOPY OF ORIENTED PURPLE MEMBRANE

KENNETH J. ROTHSCHILD, *Department of Physics and Department of Physiology, Boston University, Boston, Massachusetts 02215*
NOEL A. CLARK, *Department of Physics and Astrophysics, University of Colorado, Boulder, Colorado 80309 U.S.A.*

ABSTRACT Polarized Fourier transform infrared spectroscopy has been used to study the structure of purple membrane from *Halobacterium halobium*. Membranes were oriented by drying a suspension of membrane fragments onto Irtran-4 slides. Dichroism measurements of the amide I, II, and A peaks were used to find the average spatial orientation of the bacteriorhodopsin α-helices. By deriving a function that relates the observed dichroism to the orientational order parameters for the peptide groups, helical axis distribution, and mosaic spread of the membranes, the average orientation of the α-helices was found to lie in a range less than 26° away from the membrane normal, agreeing with electron microscopic measurements. The frequency of the amide I and A peaks is at least 10 cm^{-1} higher than values found for most α-helical polypeptides and proteins. This may indicate that bacteriorhodopsin contains distorted α-helical conformations.

INTRODUCTION

The purple membrane of *Halobacterium halobium* contains a single membrane protein, bacteriorhodopsin, crystalized in the bilayer plane as a two-dimensional hexagonal array (1, 2). Much interest has been focused on the structure of this protein because it has been shown to function as a light-driven proton pump (3–5). Henderson and Unwin have recently shown by electron diffraction that this protein consists largely of seven rods of high electron density that run transversely through the bilayer plane (6). X-ray diffraction data (7, 8) indicate that these rods are α-helices.

In this paper we report on the use of polarized infrared (IR) spectroscopy to study dried, oriented films of purple membrane. This study was motivated by the ability of vibrational spectroscopy to probe the composition and structure of membranes (9–13), and the successful application of IR dichroism to determine the structure of oriented macromolecular systems (14–17). Purple membrane presents an opportunity to study the IR dichroism of an oriented preparation of a single membrane protein *in situ*. Measurements of linear IR dichroism have been used to determine the orientational order parameter of the bacteriorhodopsin α-helices relative to the sample plane. Measurements of peak frequency gave additional information about overall hydrogen bonding in these α-helices and other structural components of the membrane.

MATERIALS AND METHODS

Purple membrane was prepared from *Halobacterium halobium* R_1 according to the method of Becher and Cassim (18). Sodium dodecylsulfate-polyacrylamide gel electrophoresis revealed a single

protein band with a mol wt ~25,000. The purple membrane was washed in distilled water by repeated pelleting and resuspension to remove residual sucrose. The resulting pellet was resuspended and dried with a stream of N_2 gas on a ½-mm thick Kodak Irtran-4 slide to form a film ≤ 1 μm thick (Eastman Kodak Co., Rochester, N.Y.). This method resulted in a preferential stacking of the membrane fragments in the plane of the slide. Freeze-fracture micrographs of dried sample revealed well-ordered lamellar stacking of membrane fragments. Birefringence measurements showed the sample was optically uniaxial with the optic axis normal to the sample plane (19). This agrees with recent linear dichroism measurements made on dried purple membrane (20).

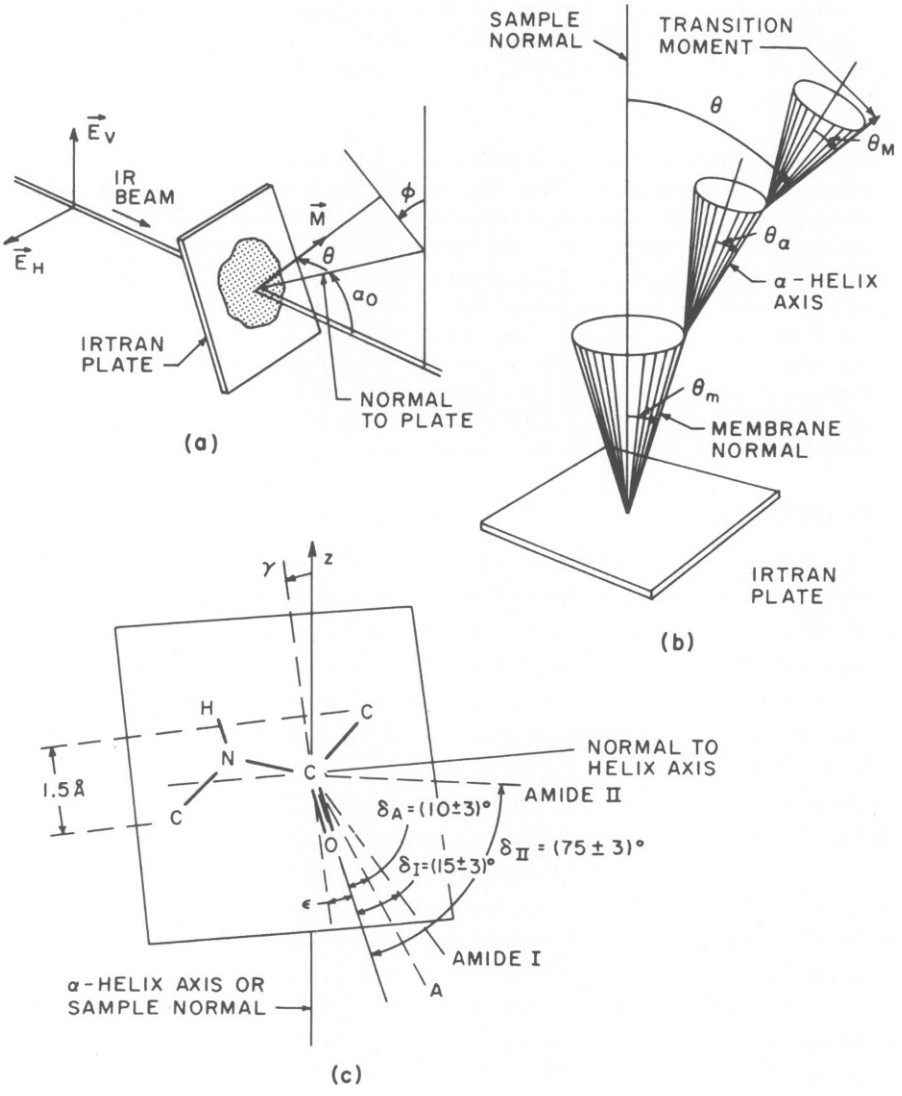

FIGURE 1 (*a*) Experimental configuration for polarized Fourier transform IR absorption measurements of purple membrane oriented on Irtran plates. (*b*) Geometry indicating a set of nested axially symmetric distributions. The moment, M, is distributed about the α-helix axis, which is distributed about the membrane normal that has a mosaic spread distribution about the sample normal. In the case of the purple membrane, the distributions are assumed to be axially symmetric. (*c*) Peptide plane geometry assumed to be the basic absorbing unit.

Polarized IR measurements were made by using a dual beam Fourier transform IR spectrometer (Digilab FTS-14, Digilab, Inc., Cambridge, Mass.). The sample was mounted in one beam on a single axis goniometer by which it could be tilted to any angle α_0 around a horizontal axis arranged normal to the incident IR beam (cf. Fig. 1 *a*). An IR polarized (PGY-Cambridge Scientific) was placed before the sample in the IR beam (Cambridge Scientific Industries Inc., Cambridge, Md.). Spectra were measured at α_0 = 0, 15, 30, 45, and 60° for the polarizer set in the horizontal position, where the incident electric vector is parallel to the plane of the slide for all α_0, and in the vertical position, where the incident electric vector makes an angle α_0 with the plane of the slide. Spectra were recorded from 400–4,000 cm^{-1} at 4 cm^{-1} resolution by using 50–100 scans of both the reference and sample beams. This allowed peak assignments to be made with an accuracy of better than ±1 cm^{-1}. Frequency calibration was made automatically with an internal He—Ne laser and was checked by using polystyrene film. Measurements were carried out on at least two different samples for each angle and polarization. Absorption spectra were determined by subtracting the logarithm of the sample beam intensity from that of the reference beam intensity to correct for the wavelength dependence of the output power of the IR source. Each absorption spectrum was then corrected by subtracting the absorption spectrum of the polarizer and appropriately oriented blank Irtran-4 slide. This procedure eliminated artifacts due to the wavelength-dependent transmission of the polarizer and Irtran in the polarized incident radiation, and yielded spectra with flat base lines (Figs. 2 and 3). Note that variations in Fresnel reflection losses with angle and polarization, which merely shift the base line, are not significant. The wavelength dependence of the Fresnel loss was neglected.

DATA

Figs. 2 and 3 show the spectra of purple membrane from 600–2,200 cm^{-1} and 2,200–3,600 cm^{-1}, respectively, for α_0 = 0, 15, 30, 45, and 60°, with the polarizer in the vertical position and horizontal position (labeled *H*). The major peaks are assigned to either vibrations of the protein (bacteriorhodopsin) or the membrane lipids (9–17) (cf. Table I). The two peaks at 1,662 and 1,545 cm^{-1} in Fig. 2 *a* (α_0 = 0) are assigned to the amide I (C═O stretch) and amide II (in-plane NH bend) vibrations (9–17, 21–28). For the horizontal polarization, the amide I and II peaks exhibit at all α_0 a high amide II/amide I peak ratio of 0.98, comparable to the more typical value of 0.45 observed in proteins (21). For the vertical polarization (Figs. 2 and 3, *A–E*) this ratio varies from 0.98 at α_0 = 0° to 0.51 at α_0 = 60°. In addition, the amide I peak shifts to 1,667 cm^{-1} as α_0 approaches 60°. A third peak near 3,300 cm^{-1} (α_0 = 0°) and 3,310 cm^{-1} (α_0 = 60°) assigned to the amide A mode (NH stretching) is also found to increase in absorbance with increasing α_0 (cf. Fig. 3). These effects are explainable only if the transition moments in purple membrane have an anisotropic orientational distribution. In this case the vectorial nature of the amide I, II, and A vibrations (14, 21–28) renders the relative peak intensities dependent on the angle the incident electric vector makes with each individual transition moment. Such an effect is found, for example, in oriented films of α-helical poly-γ-benzyl-L-glutamate (27). Fig. 4 shows the difference spectrum obtained by subtracting the spectrum for vertical polarization at α_0 = 45° from the vertical polarization at 0°. The negative peaks at 1,667 and 3,312 cm^{-1} indicate increased dichroism, whereas a positive peak at 1,545 cm^{-1} indicates a decreasing dichroism of the amide I, A, and II peaks, respectively.

THEORY AND ANALYSIS

To analyze these data, we calculate the dichroic ratio *R* as measured for the geometry of Fig. 1 *a*:

$$R = \langle(\mathbf{E}_V \cdot \mathbf{M})^2\rangle_{f(\theta)} / \langle(\mathbf{E}_H \cdot \mathbf{M})^2\rangle_{f(\theta)}, \quad (1)$$

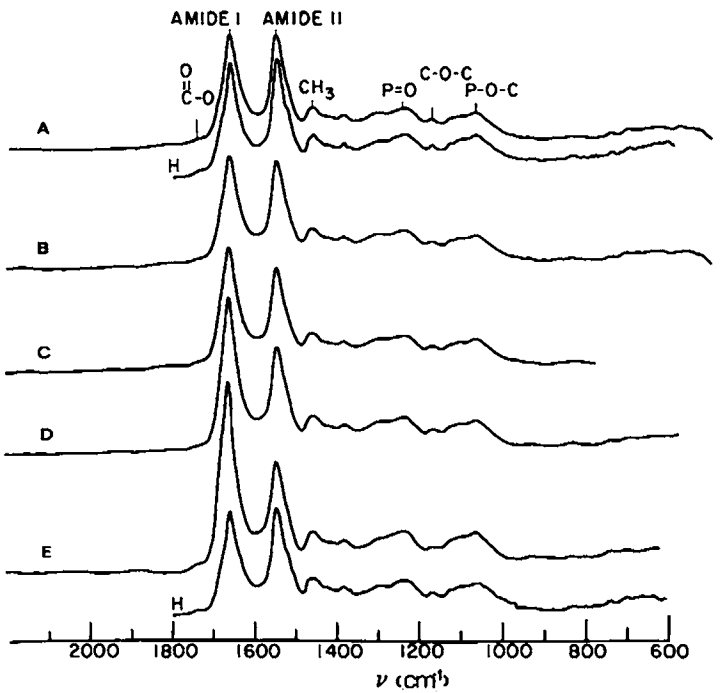

FIGURE 2

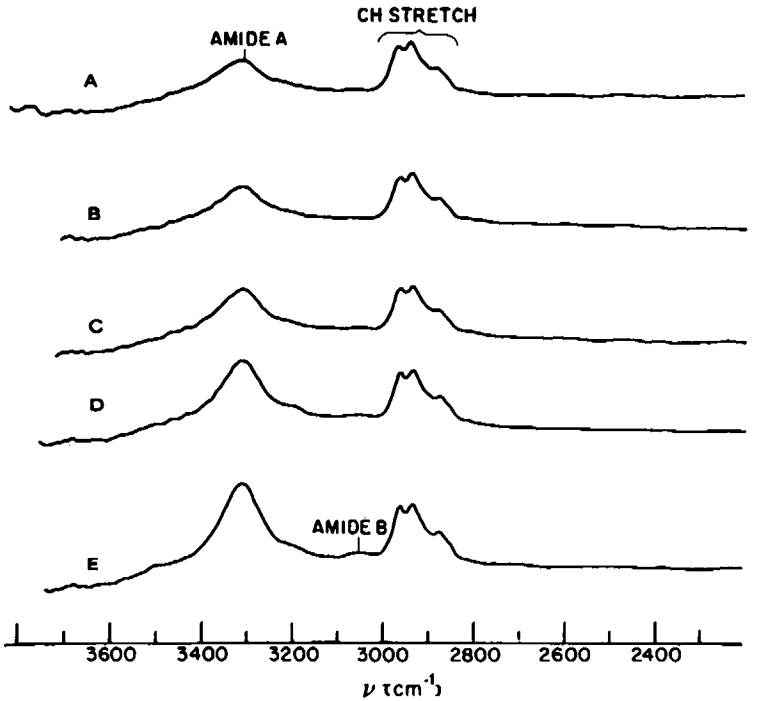

FIGURE 3

FIGURE 2 Dichroic IR absorption of dried purple membrane on Irtran-4 slide from 600 to 2,200 cm^{-1}. Vertical (absorbance), horizontal axis (wave numbers, cm^{-1}). Spectra were recorded with 100 scans of sample and 50 scans of reference beam at a resolution of 4 cm^{-1}. Optical densities ranged from 0 to a maximum of 1. A polarizer was placed before the sample in either a vertical or horizontal polarization (denoted *H*) and the sample tilted on a single axis goniometer at an angle α_0, relative to the vertical polarization. Spectra were obtained for α_0 = 0, 15, 30, 45, and 60°, as shown in Fig. 2 *A–E*, respectively. All spectra were made by subtracting the absorption of the polarizer and blank slide. Vertical spectra were smoothed by using a nine-point Lorentzian smoothing factor.

FIGURE 3 Same as Fig. 2. Spectra from 2,200–3,800 cm^{-1}.

TABLE I

FREQUENCY OF PEAKS IN IR ABSORPTION SPECTRUM OF PURPLE MEMBRANE FROM 500 TO 3,600 cm^{-1}.

$\nu(cm^{-1})$	Assignment	Dichroism
577	Amide VI (out-of-plane deformation)	
590 (s)		∥
605-665 (B)		
610		
700	Phenyl B_2	
740	CH (rocking), amide V (?)	
825 (B)		∥
937 (w)		∥
975 (w)	C—O stretching (perpendicular)	⊥
1,062	P—O—C stretching	
1,100		
1,125		
1,167	Ester carbonyl stretch, CH_3	
1,235	P═O stretch	
1,300		
1,367 (s)	CH_2 wag	
1,382		
1,415 (w)	CO_2 stretch (Glu, Asp)	
1,457	CH_3 bending modes	
1,515 (s)	Tyrosine	
1,547	Amide II	⊥
1,661	Amide I ($\alpha_0 = 0°$)	⊥
1,667	Amide I ($\alpha_0 = 60°$)	∥
	O ‖	
1725 (w)	C—OH (Glu, Asp)	
1,740	Ester carbonyl stretch	
2,850 (s)	CH stretching modes	
2,870		
2,929		
2,958		
3,060	Amide B	∥
3,310	Amide A	∥

Tentative assignments were made from references (9, 11-17, 21-27, 34). The type of dichroism found is indicated by ∥ (absorption greatest at $\alpha_0 = 90°$), ⊥ (absorption greatest at $\alpha_0 = 0°$). Other symbols referring to the appearance of peaks are s (shoulder), w (weak), and B (broad). Peak frequencies were measured directly from spectra and found to vary no more than ± 1 cm^{-1} for different samples.

where **M** is a vectorial transition moment, and the average is over the distribution $f(\theta, \phi)$ of orientations of **M**. We assume the sample to be isotropic with respect to orientatio in the plane (f independent of ϕ) and with respect to a $\pm\pi$ change in α_0 [as many membranes face up as face down, $f(\theta) = f(\pi - \theta)$]. The distribution $f(\theta)$ may then be written as a sum of even Legendre polynomials:

$$f(\theta) = \sum_{n=0} [(4n + 1)/2] < P_{2n}(\cos\theta) > P_{2n}(\cos\theta), \qquad (2)$$

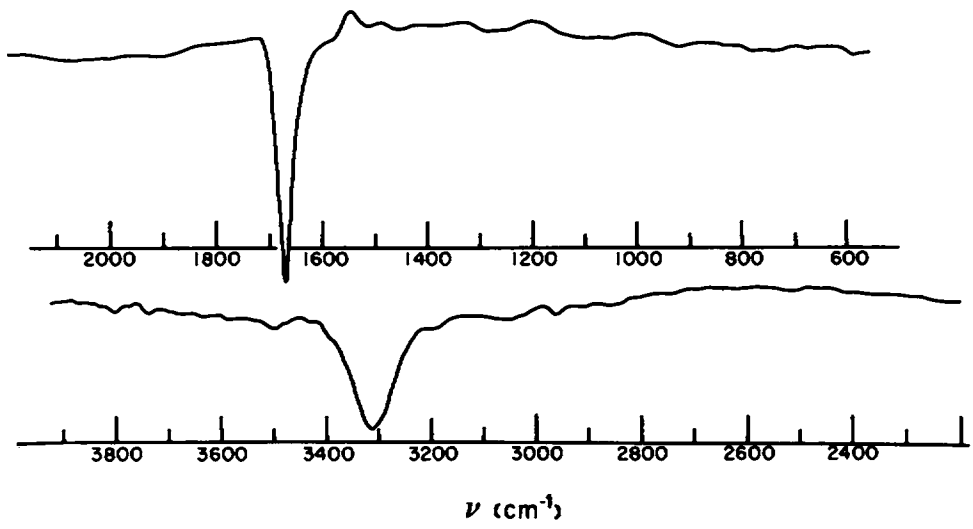

FIGURE 4 A plot of the vertical absorbance at $\alpha_0 = 45°$ subtracted from the vertical absorbance at 0° vs. wave number. The major difference peaks occur at 1,667 cm^{-1} (R = 1.4), 1,545 cm^{-1} (R = 0.93), and 3,310 cm^{-1} (R = 1.82).

where P_l is the Legendre polynomial of order l ($P_0 = 1$, $P_2 = (3\cos^2\theta - 1)/2, \ldots$), and:

$$<P_{2l}>_{f(\theta)} = \int_0^{\pi} \sin\theta d\theta P_{2l}(\cos\theta) f(\theta). \tag{3}$$

Under these conditions the dichroic ratio is given by

$$R = 1 + \sin^2\alpha(3<P_2>_{f(\theta)}/[1 - <P_2>_{f(\theta)}]). \tag{4}$$

(Eq. 4 reduces to Eq. 14 of ref. 15 when the transition moment **M** is assumed to make an angle θ with the sample normal.) Here α is the angle between $\mathbf{E}_\nu$ and the sample plane (cf. Fig. 1) and is given by Snell's law, $\alpha = \sin^{-1}(\sin\alpha_0/n)$, where n is the sample refractive index. (We ignore the weak optical anisotropy.) Eq. 4 shows that in general R vs. $\sin^2\alpha$ should yield a linear plot with unit intercept and a slope determined by $<P_2>_f = <(3\cos^2\theta - 1)/2>_f$, the only moment of the distribution f to influence the dichroism.

We now relate $<P_2>_f$ to the membrane structure. We consider the basic absorbing entity to be the planar peptide group shown in Fig. 1 *c*. The transition moments for the amide, I, II, and A vibrations lie parallel to the peptide plane and are oriented as indicated at angles

$$\delta_A = (10 \pm 3)°, \quad \delta_I = (15 \pm 3)°, \quad \text{and} \quad \delta_{II} = (75 \pm 3)°, \tag{5}$$

respectively, from the C=O bond direction (26–28). We may calculate $<P_2>_f$ for a given vibration by assuming a distribution $f(\eta, \gamma_n, \epsilon_n)$ of the peptide plane orientation, where η, γ_n, ϵ_n are the Euler angles giving the peptide plane orientation about the sample normal. If the sample is macroscopically isotropic, $f(\eta, \gamma_n, \epsilon_n)$ is independent of η (which is therefore not shown) and depends only on the angles γ_n and ϵ_n, where γ_n is the tilt of a particular peptide plane from the sample normal. For the geometry indicated in Fig. 1 *c*, $<P_2(\theta)>_f$ of a particular vibration may be expressed as follows in terms of the moments of $f(\gamma_n, \epsilon_n)$ by using $\cos\theta = \cos\gamma_n\cos(\epsilon_n + \delta_n)$:

$$<P_2>_f = \tfrac{3}{2}\{<\cos^2\gamma_n\cos^2\epsilon_n>\cos^2\delta_M + <\cos^2\gamma_n\sin^2\epsilon_n>\sin^2\delta_M - 2<\cos^2\gamma_n\cos\epsilon_n\sin\epsilon_n>\cos\delta_M\sin\delta_M\} - \tfrac{1}{2}. \quad (6)$$

Since $<P_2>_f$ is measurable for three vibrations of the peptide plane, Eq. 6 may be written for each δ and the resulting equations solved for the three averages:

$$\begin{aligned} a_1 &= <\cos^2\gamma_n\cos^2\epsilon_n> \\ a_2 &= <\cos^2\gamma_n\sin^2\epsilon_n> \\ a_3 &= <\cos^2\gamma_n\cos\epsilon_n\sin\epsilon_n> \\ <\cos^2\gamma_n> &= a_1 + a_2. \end{aligned} \quad (7)$$

In general, variations in γ and ϵ will be correlated so that, for example, $<\cos^2\gamma_n\cos^2\epsilon_n> \neq <\cos^2\gamma_n><\cos^2\epsilon_n>$, and evaluation of the angle $<\cos^2\epsilon>$ is not possible without knowledge of the joint distribution $f(\gamma, \epsilon)$.

Although a_1, a_2, and a_3 may in principle be calculated from three measurements of $<P_2>_f$, in practice errors in the $<P_2>_f$ data produce large uncertainty in the a_i, making them of qualitative use only. However, useful information concerning the distribution of moments is obtainable if we consider a more restrictive model for the orientation distribution. We assume in what follows that the membrane protein is entirely α-helical with fixed γ_M and ϵ_M relative to a local α-helical axis. We assume $f(\theta)$ to be determined by a set of nested axially symmetric distributions, as illustrated in Fig. 1*b*. The transition moment M has an axially symmetric distribution $f_M(\theta_M)$ determined by γ_M and ϵ_M about the α-helix axis, which is in turn isotropically distributed about the membrane normal with $f_\alpha(\theta_\alpha)$. Since there may not be perfect orientation of the purple membrane fragments, we distribute the membrane normals with a mosaic spread function $f_m(\theta_m)$, again assumed to be axially symmetric. With this model, the measured moment $<P_2>_f$ of the distribution about the normal to the Irtran plate reduces to:

$$<P_2> = <P_2>_{f_m}<P_2>_{f_\alpha}<P_2>_{f_M}. \quad (8)$$

This follows from application of the addition theorem of spherical harmonics (29). Eq. 4 now describes the dichroism for any nested set of axially symmetric distributions.

The average $<P_2>_{f_M}$ depends on the angles γ_M and ϵ_M that, as shown in Fig. 1*c*, describe the orientation of the peptide group relative to the α-helix axis, and on δ, which mea-

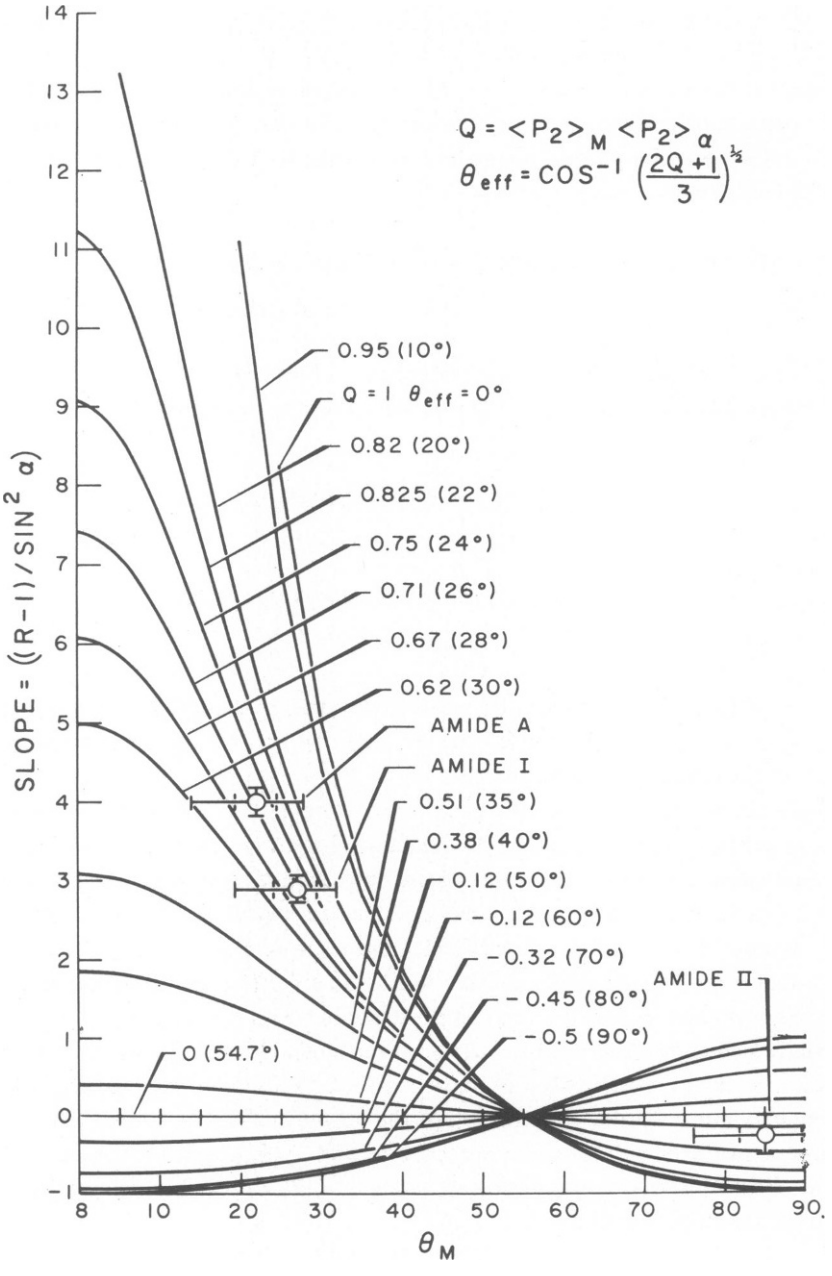

FIGURE 5 The slope of $R(\sin^2\alpha)$ for an absorption dipole, M, vs. θ_M, the angle between M and an axis about which M is symmetrically distributed for various values of Q (the order parameter for the symmetric distribution of the axis about the sample normal). The error bars are due to the variability in measurements made for θ_M, as well as variability in peak intensity.

sures the angle the transition moment makes with the C=O group. The angles γ_M and ϵ_M will depend to some extent on the constituents of the helix, but are expected to normally lie well within the range $0 < \gamma_M < 10°$ (27), and $7 < \epsilon_M < 13°$ (14). Using these ranges and Eq. 5, we find the following angles, θ_M, for the principal peptide transition moments:

$$\theta_A = \begin{pmatrix} 22 & +7 \\ & -8 \end{pmatrix}^\circ$$

$$\theta_I = \begin{pmatrix} 27 & +5 \\ & -7 \end{pmatrix}^\circ$$

$$\theta_{II} = \begin{pmatrix} 85 & +5 \\ & -9 \end{pmatrix}^\circ. \tag{9}$$

To obtain $<P_2>_{f_m}$, we assume $f_M(\theta_M)$ to be a δ function, so that $<P_2>_{f_M} = P_2(\cos\theta_M)$, where θ_M can vary over the indicated range in Eq. 9. Defining $Q \equiv <P_2>_{f_m}<P_2>_{f_\alpha}$, we rewrite Eq. 8 as

$$<P_2>_f = QP_2(\cos\theta_M). \tag{10}$$

In Fig. 5 we have plotted the slope ($S = 3<P_2>_f/(1 - <P_2>_f)$ of R vs. $\sin^2\alpha$ (Eq. 4) as a function of θ_M for various values of $Q = <P_2>_{f_m}<P_2>_{f_\alpha}$. Q may be viewed as an orientational order parameter for the α-helix axes relative to the sample normal. We have also indicated the effective tilt angle, θ_{eff}, which the α-helix would have in order to produce a particular Q. If for a given Q there were no mosaic spread ($<P_2>_{f_m} = 1$) and all the α-helix axes were tilted from the normal by the angle, then θ_{eff} would be given by: $\theta_{eff} = \cos^{-1}((2Q + 1)/3)^{1/2}$. Fig. 5 illustrates the behavior expected in tilted sample dichroism measurements. For moments nearly parallel to the sample normal ($Q \cong 1$, $\theta_M \cong 0$), the slope and the dichroism are large. For $Q \cong 1$ and $\theta_M \cong 90°$ or $Q \cong -\frac{1}{2}$, $\theta_M \cong 0$ (M distributed in the membrane plane), the slope is negative, as would be expected qualitatively. For $Q = 0$ and $S = 0$ ($R = 1$) an isotropic distribution is found.

TABLE II

THE ABSORPTION INTENSITY OF THE AMIDE I, II, AND A PEAKS MEASURED AT PEAK MAXIMUM AFTER SUBTRACTING BASE LINE ABSORBANCE FOR BOTH HORIZONTAL (H) AND VERTICAL (V) POLARIZATION.

α_0	I_V	I_H	II_V	II_H	A_V	A_H
0	53	53	50.6	52.1	13.1	12.4
15	52.5	51	47.1	49.6	14.2	12.6
30	58	50.5	45.4	49.1	16.6	12.1
45	73.5	50.5	47	49.3	21.6	11.9
60	87.5	49	48	47.8	28.1	13.8
70	97	50.4	46.1	49.6	27.5	12.2

The amide II peak intensity was corrected for error due to overlap with the amide I peak by fitting the amide I to a Lorentzian. Similar overlap corrections to the amide A and amide II intensity were not significant.

RESULTS AND DISCUSSION

The amide I, II, and A peaks, by virtue of their intensity, were suitable for quantitative analysis. The dichroic ratio R was measured for various values of α (Table II). These were calculated from peak intensities corrected for overlap of distinguishable adjacent peaks by assuming Lorentzian line shapes. In each case the entire absorption was considered due to peptide vibrations. Fig. 6 shows the plots of R vs. $\sin^2\alpha$ for the amide I, II, and A vibrations. In calculating α, the refractive index of the protein layer was taken to be n = 1.7, a value typically found for polypeptides in the IR (30). Although this is little better than a guess at the refractive index for purple membrane, which appears weakly uniaxial from optical measurements (19), the calculated order parameter Q is relatively insensitive to n, such that a $\pm 20\%$ variation in n will not substantially alter conclusions to be made. Least square fits of these data to Eq. 4 (straight lines with unit intercept) yielded the following slopes and $<P_2>_f$ for the three moments:

$$\begin{aligned}
&\text{Amide A:} \quad \text{slope} = 3.99 \pm 0.16 \qquad <P_2>_f = 0.570 \pm 0.10 \\
&\text{Amide II:} \quad \text{slope} = -0.23 \pm 0.15 \qquad <P_2>_f = -0.083 \pm 0.06 \\
&\text{Amide I:} \quad \text{slope} = 2.87 \pm 0.20 \qquad <P_2>_f = 0.488 \pm 0.01. \qquad (11)
\end{aligned}$$

We may use these values of $<P_2>$ and the δ_A, δ_I, and δ_{II} values of Eq. 5 to calculate the averages a_1, a_2, and a_3 of Eq. 7. As mentioned above, errors in the a_i are large, with $0.86 < <\cos^2\gamma> < 1.12$ and $0.74 < a_1 = <\cos^2\gamma\cos^2\epsilon> < 0.85$ (clearly only $\cos^2\gamma < 1$ is physically reasonable). Hence, qualitatively it is clear that both γ and ϵ are small ($\gamma, \epsilon \lesssim 20°$), agreeing with previous IR dichroism studies on oriented α-helical polypeptides (14, 27).

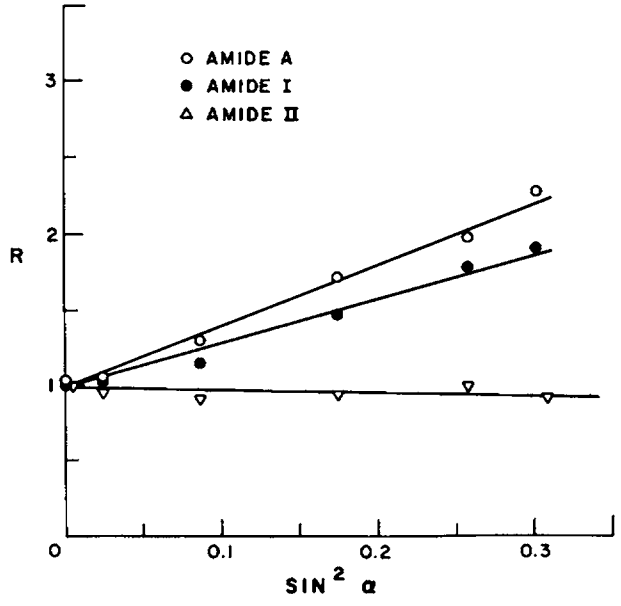

FIGURE 6 Measurement of dichroic ratio, R, for the amide I, II, and A vibrations, showing the expected linear dependence on $\sin^2\alpha$. The three slopes are shown in Fig. 5.

To use the measured $<P_2>_f$ in the framework of the nested axis model, we plot in Fig. 5 the slope for the amide I, II, and A vibrations, using the respective θ_M ranges given in Eq. 9 to determine the abscissa. If the nested model is correct, then the three resulting points should all lie on a curve of common Q. Note that the amide A and I points fall on the $Q = 0.71$ ($\theta_{eff} = 26°$) curve that is close to but out of the range of the amide II error bars. If we consider the common curves for the amide I and A points, the data indicate a range for Q and θ_{eff} of $0.6 < Q < 0.8$ and $20° < \theta_{eff} < 32°$, respectively. The largest contribution to the uncertainty in Q and θ_{eff} is the θ_M ranges in Eq. 9. These can be reduced by application of the results of other experiments. For example, X-ray diffraction has shown the α-helices in bacteriorhodopsin to have an advance per residue $h = (1.50 \pm 0.03)$Å. From the geometry of the peptide group of Fig. 1 *c* the ϵ_M spread in Eq. 9 yields h in the range 1.2Å $< h <$ 2.2Å. If we constrain ϵ_M using the above X-ray data, the ranges for possible variation in Eq. 9 are reduced by two-thirds and the corresponding Q and θ_{eff} ranges for the amide A and I data from Fig. 5 are $0.67 < Q < 0.75$ and $24° < \theta_{eff} < 28°$.

There are several possible explanations for the amide II slope falling outside the range of the common Q curve for the amide I and A points. We consider below two of the more likely possibilities. *a*) The existence of a nondichroic peak near the amide II frequency is indicated by the shoulder appearing on the low wave number side of this peak. This would add a constant component to the peak intensity and make the dichroism appear smaller, hence shifting the slope to lower values. *b*) A portion of the bacteriorhodopsin polypeptide chain may be non-α-helical. Although estimates of the bacteriorhodopsin α-helical content based on the Henderson-Unwin model (6) range up to 80%, a recent ultraviolet-circular dichroism study estimated the α-helical content at only 40% (31). Nonhelical components of the protein will affect our results in several possible ways. For example, if we assume that 20% of the peptide groups are oriented with $\gamma = 0°$ and $\epsilon = -12°$, the slopes of the amide I, II, and A peaks calculated for the α-helical distribution would intersect the $Q = 0.62$ ($\theta_{eff} = 30°$) curve within the limits of error. On the other hand, if we assume there is approximately a 50% nondichroic component in each peak, all three points fall near the $Q = 0.82$ ($\theta_{eff} = 20°$) curve.

Keep in mind that Q is determined both by the mosaic spread and the intrinsic α-helix distribution. A rough estimate of the mosaic spread is obtainable from freeze-fracture observations of multilayer-oriented samples (19). Study of fracture faces normal to the membrane planes shows these planes are highly oriented and that the mosaic spread is caused largely by distortion of the layered structure around foreign particles. Distribution of membrane orientations obtained from such fracture faces indicates that $<P_2>_{f_m} \sim 0.9$. Linear dichroism measurements at 565 nm also reveal little mosaic spread. The intrinsic α-helix distribution order parameter would then be $<P_2>_{f_\alpha} \geq 0.8$ ($\theta_{eff} \lesssim 21°$). Neutron diffraction of purple membrane dried on quartz plates has also indicated only a small amount of mosaic spread (20).

The Henderson-Unwin electron microscopic-determined picture of bacteriorhodopsin shows three α-helical segments perpendicular to the plane of the membrane and four inclined at a small angle. If we assume that our measurements include three absolutely perpendicular segments, then the other four segments would have to be inclined at an average tilt no greater than 28°.

Frequency of the Amide A, I, and II Bands

Numerous experimental and theoretical studies have established that a rough correlation exists between the frequency of specific peptide group vibrations and the secondary structure of a protein (14–17, 21–28). It has been found that the amide I and II vibrations for a wide variety of extensively α-helical polypeptides and proteins fall in the range 1,650–1,655 cm^{-1}, although one must use the amide I frequency as a sign of α-helical structure with caution, since unordered conformation also falls near 1,656 cm^{-1} (23).

Both the amide A and amide I bands of bacteriorhodopsin fall outside the normal range for an α-helix. The amide I approaches 1,667 cm^{-1} and the amide A 3,312 cm^{-1} as $\alpha \rightarrow 70°$. While this deviation could be attributed to drying of the membrane, randomly oriented suspensions of membrane fragments in D_2O still display an amide I peak at 1,660 cm^{-1}. Hence, it is likely that the high amide I frequency reflects a structural feature of the native purple membrane.

Several factors might contribute to the abnormally high amide I and amide A frequencies:

(*1*) It is likely that significant distortion from the standard Pauling-Corey α-helix (pitch, P = 5.4 Å and unit height, h = 1.5 Å) will produce shifts from the normal amide I and A frequencies of an α-helix. For example, weakening of hydrogen bond strength normally raises the amide I and A frequency (33, 34) of peptide groups, although one must use caution in extrapolating this effect to α-helices. Two examples of distorted α-helical polypeptides with amide I frequencies near 1,665 cm^{-1} are poly-β-benzyl-L-aspartate, which forms a left-handed helix (35), and poly-β-benzyl-D-L-glutamate, which forms an $\alpha_{D,L}$-helix (36). In the case of bacteriorhodopsin, the existence of distorted α-helical conformation is also supported by X-ray scattering on dried purple membrane, which reveals an anomalous pitch, P = 5.05 Å(7).

Two possible explanations for distorted α-helices in bacteriorhodopsin are the existence of supercoiling, as reported (6), or an unusual primary sequence that promotes the specific interactions of side-groups, thereby disrupting the normal α-helical conformation. In fact, both side-group interactions and supercoiling have been proposed as part of a mechanism for proton transport in bacteriorhodopsin (37). Recent partial amino-acid sequencing of bacteriorhodopsin (90 residues) also reveals that the sequence occurring in the α-helical region is atypical for an α-helix (38).

(*2*) Other membrane groups might contribute to the absorption near 1,665 cm^{-1}, thereby raising the apparent position of the amide I frequency. These include retinal, the bacteriorhodopsin chromophore found to absorb near 1,665 cm^{-1}, the guanidinium groups of arginine and lysine, and perhaps some of the unusual triglycosyl diether and glycosulfate lipids found in purple membrane (39). However, since a large dichroism is observed at 1,667 cm^{-1}, the absorbing group must be both one of the most intense vibrations in the membrane as well as highly dichroic. It is unlikely that the above groups are present in sufficient quantity in relation to the protein peptide groups to account for this degree of dichroism.

(*3*) The shift of the amide I band from 1,660 cm^{-1} to 1,665 cm^{-1} might reflect a shift between the two IR-active amide I modes predicted for the carbonyl groups in an α-helix (9, 14, 16). However, it can be shown that of these two modes, the perpendicular component (α_0 = 0) to the alpha-helix axis should be at a higher frequency (14). This contra-

dicts our measurements, indicating the parallel component (α_0 = 90) is near 1,665 cm^{-1}. More likely, the activity near 1,660 cm^{-1}, emphasized in the perpendicular orientation, is due to predominantly unordered conformation for which ν_1 = 1,656 cm^{-1} (23). Unfortunately, it is difficult to resolve this component, which is obscured by the α-helical amide I contribution to bacteriorhodopsin.

Other Membrane Groups

Several other peaks in Figs. 2 and 3 can be tentatively assigned to either lipid or protein groups in the membrane (Table I) (9, 11–17, 21–27, 36). Prominent peaks appear at 1,235 cm^{-1} (P=O), 1,062 cm^{-1} (P—O—C stretch), and 1,167 cm^{-1} (C—O—C stretch), which are likely to be part of the phospholipid content of the membrane, estimated to be only 25%. The ester carbonyl stretch peak (1,740 cm^{-1}) that appears as a strong band in the IR spectrum of most membranes (9, 11–13) appears only weakly in purple membrane, due to the unusually low lipid content. It is usually difficult to detect protein residue vibrations because they are obscured by other modes. The shoulder near 1,515 cm^{-1} may be due to tyrosine (40), although the perpendicular component of the amide II also absorbs in this region.

Limitations of the Present IR Measurements on Purple Membrane

The measurements made thus far are for the light-adapted form of purple membrane. It would be desirable to measure IR spectra under conditions where the membrane is partially or completely trapped in 412 mm intermediate.

In this study we approximated the integrated intensity by measuring peak height corrected in the case of the amide II for overlap with the amide I peak. A more complete analysis would attempt a complete deconvolution of overlapping peaks and measurement of actual integrated intensity.

These studies were performed in most part on dried purple membrane, as were some X-ray measurements (7) and the electron microscope studies of Henderson and Unwin (6) (in this case the membranes were dried in sucrose solutions). We have also studied membranes dried from 0.1 M sucrose solutions. Although much H_2O absorption is present near the amide I peak, under these conditions it can be subtracted, revealing an amide I frequency of 1,665 cm^{-1}.

In conjunction with the present study, we also studied the dried bacteriorhodopsin film using resonance Raman spectroscopy and optical birefringence measurements. We observed little difference in the Schiff base region of the 412 nm intermediates between the dried and aqueous suspended membranes, establishing that the 570 mm intermediate contains a protonated Schiff base, and the 412 mm intermediate an unprotonated Schiff base in the dried state, as has been found in the suspended state (41, 42).[1] The dried film also exhibited optical transmittance changes upon exposure to light, which could be interpreted as due to a transition between two different states. The decay of the light-driven state (presumably the 412 mm intermediate) occurred slowly with a time constant $\approx$ 1 s, agreeing with a previous report (43).

[1]Rothschild, K. J., N. A. Clark, and P. Argade. Work in preparation.

Conclusions

Polarized IR measurements of purple membrane confirm the electron microscope determined model of bacteriorhodopsin that consists largely of α-helices running transverse to the bilayer plane. We find an amide A and I frequency outside the normal range of most α-helical proteins and polypeptides. These frequency shifts may be a consequence of the α-helix distortion found by Henderson in his X-ray study of purple membrane. The application of some of the methods reported here should be useful for studying *in situ* orientation and structure of other membrane proteins such as rhodopsin.

Purple membrane preparations were generously supplied by B. Becher and T. Ebrey of the University of Illinois. Fourier transform-infrared measurements were made at the Center for Material Science at Massachusetts Institute of Technology. We also acknowledge helpful discussions with P. Argade, V. Culbertson, W. DeGrip, K. Dunker, L. Duong, T. Hsaio, J. Korenbrot, D. Luippold, P. Pershon, R. Sanches, B. Simon, and H. Stanley.

This work was supported by a grant from the National Institute of Health (National Eye Institute). Work carried out in part at the Gordon McKay Laboratory of Harvard University was supported by National Science Foundation contracts.

Received for publication 8 April 1978 and in revised form 2 September 1978.

REFERENCES

1. BLAUROCK, A. E., and W. STOECKENIUS. 1971. Structure of the purple membrane. *Nature (Lond.).* **233**:152–154.
2. STOECKENIUS, W. 1976. The purple membrane of salt-loving bacteria. *Sci. Am.* **23**:38–46.
3. OESTERHELT, D., and W. STOECKENIUS. 1973. Functions of a new photoreceptor membrane. *Proc. Natl. Acad. Sci. U. S. A.* **10**:2853–57.
4. KANNER, B. I., and E. RACKER. 1975. Light-dependent proton and rubidium translocation in membrane vesicles from *Halobacterium halobium*. *Biochem. Biophys. Res. Commun.* **64**:1054.
5. STOECKENIUS, W., and LOZIER, R. H. 1974. Light energy conversion in *Halobacterium halobium*. *J. Supramol. Struct.* **2**:769–774.
6. HENDERSON, R., and P. N. T. UNWIN. 1975. Three-dimensional model of purple membrane obtained by electron microscopy. *Nature (Lond.).* **257**:28–32.
7. HENDERSON, R. 1975. The structure of the purple membrane from Halobacterium halobium: analysis of the x-ray diffraction pattern. *J. Mol. Biol.* **93**:123–138.
8. BLAUROCK, A. 1975. Bacteriorhodopsin: A trans-membrane pump containing α-helix. *J. Mol. Biol.* **93**:139 158.
9. PARKER, F. S. 1971. Applications of Infrared Spectroscopy in Biochemistry Biology and Medicine. Plenum Publishing Corporation, New York. 601.
10. ROTHSCHILD, K. J., J. R. ANDREW, W. J. DEGRIP, and H. E. STANLEY. 1976. Opsin structure probed by Raman spectroscopy of photoreceptor membranes. *Science (Wash. D.C.).* **191**:1176–1178.
11. CHAPMAN, D., V. B. KAMAT, and R. J. LEVINE. 1968. Infrared spectra and the chain organization of erythrocyte membranes. *Science (Wash. D.C.).* **160**:314–316.
12. WALLACH, D. F., and P. H. ZAHLER. 1968. Infrared spectra of plasma membrane and endoplasmic reticulum of Ehrlich ascites carcinoma. *Biochim. Biophys. Acta.* **150**:186–193.
13. CHAPMAN, D. 1965. The Structure of Lipids. John Wiley & Sons, Inc., New York. 323.
14. FRASER, R. D. B., and T. P. MACRAE. 1973. Conformation in Fibrous Proteins and Related Synthetic Polypeptides. Academic Press, Inc., New York. 628.
15. AKUTSU, H., Y. KYOGOKU, H. NAKAHARA, and K. FUKUDA. 1975. Confrontational analysis of phosphotidylethanolamine by IR dichroism. *Chem. Phys. Lipids.* **15**:222–242.
16. FRASER, R. D. B., and E. SUZUKI. 1970. The Physical Principles and Techniques of Protein Chemistry. S. J. Leach, editor. Vol. B. Academic Press, Inc., New York. 213.
17. SUSI, H. 1969. Structure and Stability of Biological macromolecules. S. N. Timasheff and G. D. Fasman, editors. Marcal Dekker, Inc., New York. 575.

18. BECHER, B., and J. Y. CASSIM. 1975. Improved isolation procedures for the purple membrane of *Halobacterium halobium*. *Prep. Biochem.* **5**:161–178.
19. SIMON, B., D. LUIPPOLD, N. A. CLARK, and K. J. ROTHSCHILD. 1978. Physical studies of oriented purple membrane. *Bull. Am. Phys. Soc.* **23**:283.
20. HEYN, M. P., R. J. CHERRY, and U. MÜLLER. 1977. Transient and linear dichroism studies on bacteriorhodopsin: determination of the orientation of the 568 nm all-trans retinal chromophore. *J. Mol. Biol.* **117**: 607–620.
21. MIYAZAWA, T., and E. R. BLOUT. 1961. The infrared spectra of polypeptides in various conformations: amide I and II bands. *J. Am. Chem. Soc.* **83**:712–719.
22. KRIMM, S. 1962. Infrared spectra and chain conformation of proteins. *J. Mol. Biol.* **4**:528–540.
23. TIMASHEFF, S. N., H. SUSI, and L. STEVENS. 1967. Infrared spectra and protein conformations in aqueous solutions. II. Survey of globular proteins. *J. Biol. Chem.* **242**:5467–5473.
24. SUSI, H., S. N. TIMASHEFF, and L. STEVENS. 1967. Infrared spectra and protein conformations in aqueous solutions. I. The amide I Band in H_2O and D_2O solutions. *J. Biol. Chem.* **242**:5460–5466.
25. BLOUT, E. R., C. DE LOZE, and A. J. ASADOURIAN. 1961. The deuterium exchange of water-soluble polypeptides and proteins as measured by infrared spectroscopy. *J. Am. Chem. Soc.* **83**:1895–1900.
26. AMBROSE, E. J., and A. ELLIOT. 1951. The structure of synthetic polypeptides. II. Investigation with polarized infrared spectroscopy. *Proc. R. Soc. (Lond.) A. Math. Phys. Sci.* **205**:47.
27. TSUBOI, M. 1962. Infrared dichroism and molecular conformation of α-form poly-γ-benzyl-L-glutamate. *J. Polym. Sci.* **58**:139–153.
28. SANDEMAN, I. 1955. Amide bands in IR spectra. *Proc. R. Soc. Lond. A. Math. Phys. Sci.* **232**:105.
29. MORSE, P. M. and H. FESHBACH. 1953. Methods of Theoretical Physics. McGraw-Hill Book Company, New York.
30. HENNIKER, C. J. 1973. Infrared refractive indices of some oriented polymers. *Macromol.* **6**:514.
31. BECHER, B., and J. Y. CASSIM. 1976. Effects of light adaptation on the purple membrane structure of *Halobacterium halobium*. *Biophys. J.* **16**:1183–1200.
32. LONG, M. M., D. W. URRY, and W. STOECKENIUS. Circular dichroism of biological membranes: purple membrane of *Halobacterium halobium*. *Biochem. Biophys. Res. Commun.* **75**:725–311.
33. PIMENTEL, G. C., and C. H. SEDERHOLM. 1956. Correlation of IR stretching frequencies and hydrogen bond distances in crystals. *J. Chem. Phys.* **24**:639–641.
34. BELLAMY, L. J. 1968. Advances in Infrared Group Frequencies. Chapman & Hall Ltd., London. 304.
35. BLOUT, E. R., and R. H. KARLSON. 1958. Poly-β-benzyl aspartates: optical rotation and the sense of the helix. *J. Am. Chem. Soc.* **80**:1259–1260.
36. HEITZ, F., B. LOTZ, and G. SPACH. 1975. α_{DL} and π_{DL} helices of alternating poly-γ-benzyl-D-L-glutamate. *J. Mol. Biol.* **92**:1–13.
37. DUNKER, A. K., and D. J. ZALESKE. 1977. Stereochemical considerations for constructing alpha-helical protein bundles with particular application to membrane proteins. *Biochem. J.* **163**:45–57.
38. OVCHINNIKOV, Y. A., N. G. ABDULAEV, M. Y. FEIGINA, A. V. KISELEV, and N. A. LOBANOV. 1977. Recent findings in the structure-functional characteristics of bacteriorhodopsin. *FEBS (Fed. Eur. Biochem. Soc.) Lett.* **84**:1–4.
39. KUSHWAHA, S. D., M. KATES, and W. G. MARTIN. 1975. Characterization and composition of the purple and red membrane from *Halobacterium cultirubrum*. *Can. J. Biochem.* **53**:284–292.
40. BENDIT, E. B. 1967. Infrared absorption of tyrosine side chains in proteins. *Biopolymers.* **5**:525–533.
41. LEWIS, A., J. SPOONHOWER, R. A. BOGOMOLNI, R. H. LOZIER, and W. STOECKENIUS. 1974. Tunable laser resonance Raman spectroscopy of bacteriorhodopsin. *Proc. Natl. Acad. Sci. U.S.A.* **71**:4462–4466.
42. MARCUS, M. A., and A. LEWIS. 1976. Kinetic resonance Raman spectroscopy: Dynamics of deprotonation of the Schiff base of bacteriorhodopsin. *Science (Wash. D.C.).* **195**:1328–1330.
43. HWANG, S. B., R. A. BOGOMOLNI, Y. W. TSENG, and W. STOECKENIUS. 1976. Angular orientation of an intermediate of the bacteriorhodopsin photochemical reaction cycle. *Biophys. J.* **17**:98*a*. (Abstr.).